

# Preparation and characterization of micro-sized $\text{FeCO}_3$ , $\text{Fe}_3\text{O}_4$ and $\text{Fe}_2\text{O}_3$ with ellipsoidal morphology

Shouhu Xuan<sup>a,b</sup>, Mingwei Chen<sup>b</sup>, Lingyun Hao<sup>b,c</sup>, Wanquan Jiang<sup>b</sup>, Xinglong Gong<sup>c</sup>,  
Yuan Hu<sup>a,\*</sup>, Zuyao Chen<sup>b</sup>

<sup>a</sup>State Key Laboratory of Fire Science, The University of Science and Technology of China (USTC), Hefei, Anhui, 230026, PR China

<sup>b</sup>Department of Chemistry, USTC, Hefei, 230026, PR China

<sup>c</sup>CAS Key Laboratory of Mechanical Behavior and Design of Materials, Department of Mechanics and Mechanical Engineering, USTC, Hefei, 230026, PR China

Received 11 October 2006; received in revised form 21 May 2007

Available online 3 June 2007

## Abstract

Ellipsoidal  $\text{FeCO}_3$  microcrystals with length of  $\sim 5\text{--}6.5\ \mu\text{m}$  and width of  $\sim 2.5\text{--}3.5\ \mu\text{m}$  have been synthesized by an ascorbic acid assisted hydrothermal process. Both micro-sized ellipsoidal  $\text{Fe}_2\text{O}_3$  and  $\text{Fe}_3\text{O}_4$  microparticles were obtained using the spindle  $\text{FeCO}_3$  as sacrificial templates via direct thermal decomposition and sealed thermal decomposition for 2 h at  $500\ ^\circ\text{C}$ , respectively. The products were characterized with the X-ray powder diffraction, scanning electron microscopy, energy-dispersive X-ray spectroscopy and superconducting quantum interference device magnetometer. The influences of the experimental factors on growth of the  $\text{FeCO}_3$  micron crystals were also investigated.

© 2007 Elsevier B.V. All rights reserved.

**Keywords:** Ellipsoidal; Magnetic; Microsized; Hydrothermal; Heating treatment

## 1. Introduction

The synthesis of inorganic materials of specific size and morphology is a key aspect in fields as diverse as modern materials, catalysis, medicine, electronics, magnetics, ceramics, pigments and cosmetics [1,2]. Therefore, studies on the shape-control synthesis of inorganic materials are of great interests and are actively pursued. During last 10 years, various shapes and morphologies such as nanocages, nanocubes and nanoboxes, nanobridges and nanonails, nanodiskettes, and star-shaped and fishbone-like structure have been successfully obtained [3–8]. Most of them are semiconductor or metal nanostructures, and only a few of them are magnetic metal oxide system in despite of their unique magnetism and important technological applica-

tions in magnetic information storage, biological tags and ferrofluids [9].

Fortunately, as iron oxides are important magnetic metal oxides, certain studies were focused on their morphologies as nanoparticles [10], nanorods [11] and hollow spheres [12], plate-shaped [13], wire-like [14] and tube-like [15] nanostructures due to their potential industrial applications in magnetic recording media, catalysts, pigments, gas sensors, optical devices, and electromagnetic devices. Non-spherical colloids and their ordered arrays may be more attractive in applications than their spherical counterparts because of their lower symmetries. Very recently, Wang et al. [16] have designed and fabricated a new rice-like hybrid nanoparticle with spindle hematite core and a continuous Au shell. They found that the plasmon tunability arising from varying the thickness of the shell layer is far more geometrically sensitive than that arising from varying the length of the nanostructure. Therefore, it is worth finding iron oxide particles with

\*Corresponding author. Tel.: +86 551 3601664; fax: +86 551 3601664.

E-mail addresses: [yuanhu@ustc.edu.cn](mailto:yuanhu@ustc.edu.cn), [shhx@mail.ustc.edu.cn](mailto:shhx@mail.ustc.edu.cn) (Y. Hu).

lower symmetries and developing new route for the synthesis of novel magnetic structures and investigation of their properties.

Ferrous carbonate is a special chemical material, which can be used as the precursor to prepare  $\text{Fe}_2\text{O}_3$  and  $\text{Fe}_3\text{O}_4$ . However, little work has been reported on the fabrication of iron oxides by this method up to now. Herein, this method was employed to synthesize  $\text{Fe}_2\text{O}_3$  and  $\text{Fe}_3\text{O}_4$  microcrystallites with ellipsoidal morphology. In this work,  $\text{FeCO}_3$  microcrystallites with ellipsoidal morphology were synthesized on the basis of controlled self-assembly by an ascorbic acid (AA) assisting hydrothermal process. Then, this ellipsoidal product was transformed to  $\text{Fe}_2\text{O}_3$  and  $\text{Fe}_3\text{O}_4$  by controlled heating treatments, respectively. To the best of our knowledge, this is the first report on the synthesis of microsized  $\text{FeCO}_3$ ,  $\text{Fe}_2\text{O}_3$  and  $\text{Fe}_3\text{O}_4$  particles with ellipsoidal morphology. The influences of the experimental factors on growth of the  $\text{FeCO}_3$  microcrystals were also investigated.

## 2. Experimental section

**Synthesis of ellipsoidal  $\text{FeCO}_3$ :** In a typical experiment,  $\text{FeCl}_3 \cdot 6\text{H}_2\text{O}$  (0.002 mol) was dissolved in 35 ml  $\text{H}_2\text{O}$  under continuously stirring to form a red solution, and then,  $\text{Na}_2\text{CO}_3$  (0.636 g) was added to the solution slowly. The 0.4 g AA was added into above solution after 10 min. After being stirred for a further 5 min, the solution was transferred and sealed in a 50 ml Teflon-sealed autoclave. The autoclave was kept at  $160^\circ\text{C}$  for 3 h before being cooled in air naturally. The final products were separated from the reaction medium by centrifugation and washed by deionized water and alcohol for several times. Then, the product was dried at  $50^\circ\text{C}$  under a vacuum oven for 12 h.

**Synthesis of ellipsoidal  $\text{Fe}_3\text{O}_4$  and  $\text{Fe}_2\text{O}_3$ :** The 25 mg of the as-prepared product was sealed in a quartz tube with 4 ml of air. Then the tube was heated to  $500^\circ\text{C}$  for 2 h in the heating rate of  $2^\circ\text{C}/\text{min}$ . For the synthesis of  $\text{Fe}_2\text{O}_3$  microcrystallites, these ellipsoidal  $\text{FeCO}_3$  particles were heated at  $500^\circ\text{C}$  for 2 h in the heating rate of  $2^\circ\text{C}/\text{min}$  under air, and the red  $\text{Fe}_2\text{O}_3$  powders were obtained. The obtained  $\text{Fe}_3\text{O}_4$  and  $\text{Fe}_2\text{O}_3$  powders were rinsed with distilled water and absolute alcohol for several times. After drying in vacuum at  $50^\circ\text{C}$  for 4 h, the products were collected for further characterization.

**Characterization:** X-ray powder diffraction (XRD) patterns of the products were obtained on a Japan Rigaku D/Max- $\gamma$ A rotation anode X-ray diffractometer equipped with graphite monochromatized Cu  $\text{K}\alpha$  radiation ( $\lambda = 1.54178 \text{ \AA}$ ). Scanning electron microscopy (SEM) images were explored on a KYKY 1010B microscope. The field emission SEM (FE-SEM) images were taken on a JEOL JSM-6700F SEM. The magnetic properties (M-H curve) were measured at room temperature on an MPMS XL magnetometer made in Quantum Design Corporation.

## 3. Results and discussions

### 3.1. Characterization of the ellipsoidal $\text{FeCO}_3$

The phase and purity of the products were first examined by XRD. Fig. 1 shows a typical XRD pattern of the as-synthesized samples, all the reflection peaks can be readily indexed to hexagonal phase of  $\text{FeCO}_3$  with lattice constants  $a = 4.69 \text{ \AA}$  and  $c = 15.37 \text{ \AA}$ , which are in agreement with the standard values (JCPDS No. 12-0531). No other phase was detected in Fig. 1, which indicated the high purity of the final products. Energy-dispersive X-ray spectroscopy (EDS) analysis (Fig. 2) confirms the pure nature of the  $\text{FeCO}_3$  product: only Fe, C and O elements were detected from the product, the atom ratio of these elements Fe: C: O is 19.85:19.69:60.47, very similar to the theory ratio 1:1:3. The EDS data is consistent with the XRD analysis and further proves the formation of pure hexagonal phase of  $\text{FeCO}_3$  product.

The morphologies and structure information were further obtained from FE-SEM. Fig. 3 provides FE-SEM images of the as-prepared  $\text{FeCO}_3$  products with ellipsoidal morphology. Fig. 3a and b are the low and high magnification FE-SEM images of the as-prepared  $\text{FeCO}_3$  ellipsoidal crystals. Fig. 3a reveals the as-prepared product consists of a large quantity of ellipsoidal  $\text{FeCO}_3$  microparticles with the typical length in range of  $\sim 5\text{--}6.5 \mu\text{m}$  and width of  $\sim 2.5\text{--}3.5 \mu\text{m}$ . Through SEM observation, the content of the ellipsoidal  $\text{FeCO}_3$  microparticles was estimated over 90% of the product. Fig. 3b presents a high-magnification SEM image of a perfect ellipsoidal  $\text{FeCO}_3$  microparticles with mean length of  $5 \mu\text{m}$  and mean width of  $2.8 \mu\text{m}$ , showing that these microparticles have smooth surfaces.

Fig. 4 represents the thermal decomposition of the  $\text{FeCO}_3$  products. The initial weight loss is mainly due to the release of water adsorbed on the surface of the product

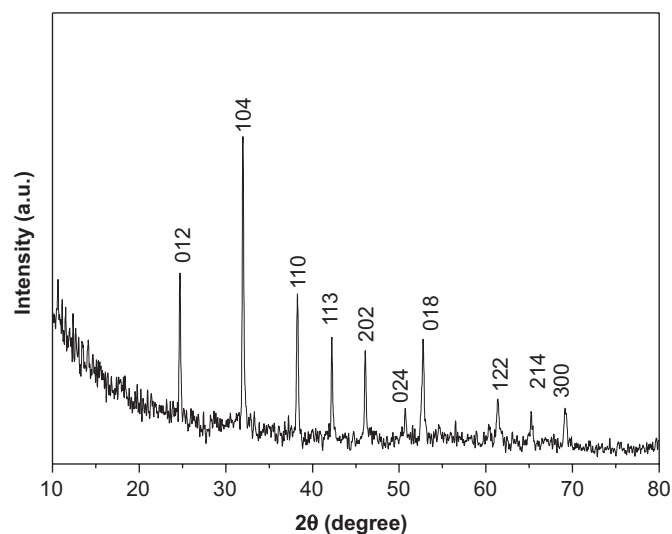
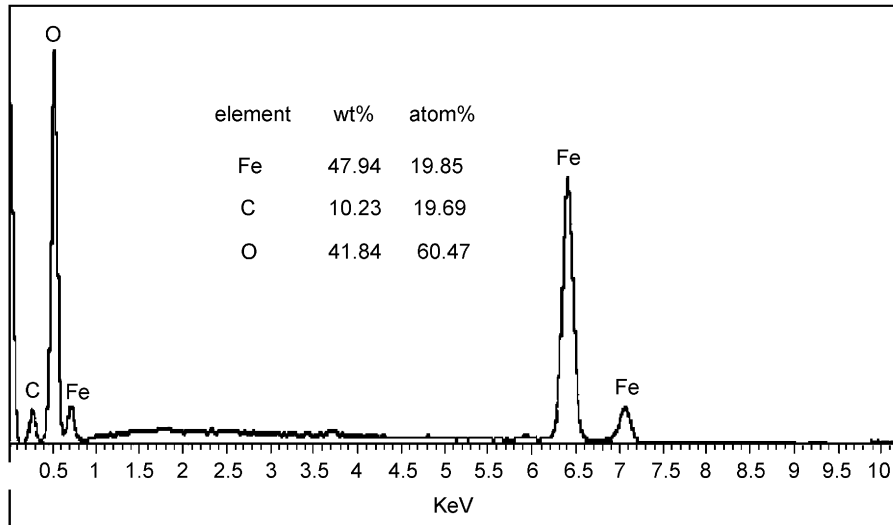
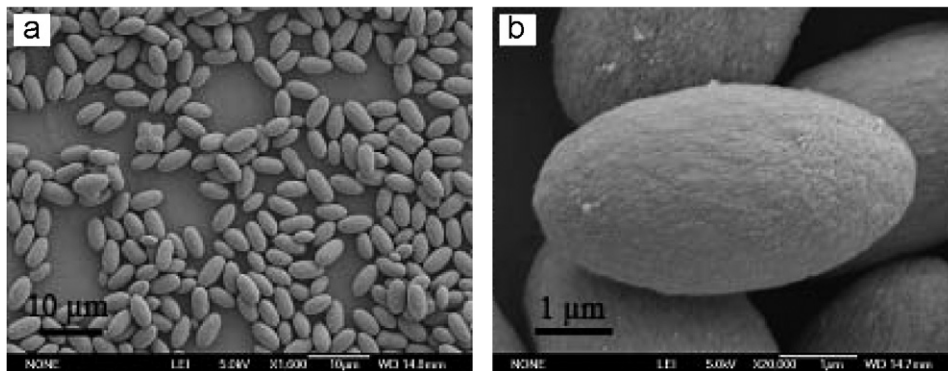
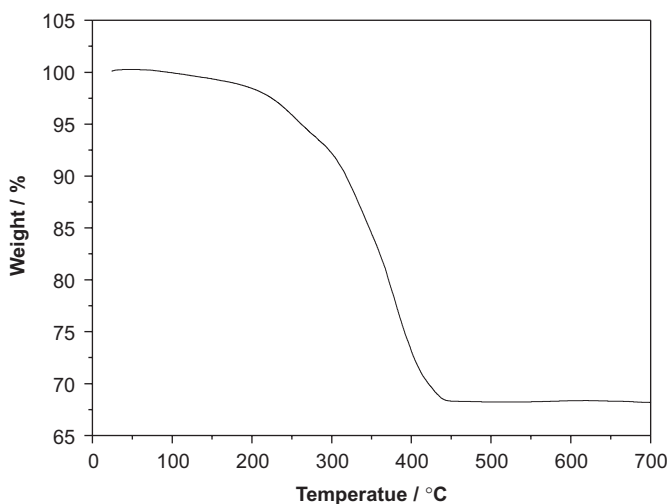


Fig. 1. XRD pattern of hexagonal  $\text{FeCO}_3$  with ellipsoidal morphology.

Fig. 2. EDS analysis of the  $\text{FeCO}_3$  product.Fig. 3. FE-SEM images of the  $\text{FeCO}_3$  with ellipsoidal morphology with low (a) and high (b) magnification.Fig. 4. TG of the  $\text{FeCO}_3$  with ellipsoidal morphology.

thermal decomposition of  $\text{FeCO}_3$ . From the TG analysis, the total weight loss is about 31.65% which is very similar to the theory date (31.03%). The TG data further support the XRD and EDS analysis results.

### 3.2. The fabrication and characterization of the ellipsoidal $\text{Fe}_2\text{O}_3$ and $\text{Fe}_3\text{O}_4$

It has been reported that the conversion of  $\text{Fe}_3\text{O}_4$  and  $\text{FeCO}_3$  into hematite is a topotactic reaction [17,18], which means that the size and shape of the starting material are preserved during the conversion. Based on this point, reactions were designed to obtain  $\text{Fe}_2\text{O}_3$  and  $\text{Fe}_3\text{O}_4$  with ellipsoidal morphology by direct thermal decomposition of ferrous carbonate under controlled conditions. In our experiment, these  $\text{FeCO}_3$  particles could be transformed to  $\text{Fe}_2\text{O}_3$  by further annealing of them at  $500^\circ\text{C}$  under oxygen atmosphere for 2 h. Fig. 5 shows the typical XRD pattern of the obtained  $\text{Fe}_2\text{O}_3$  products. All of the observed peaks of the pattern in the figure can be indexed to hexagonal phase of  $\text{Fe}_2\text{O}_3$  (JCPDS No. 86-0550). No other impurities

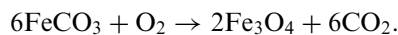
and the slow decomposition of the  $\text{FeCO}_3$  at lower temperature. A sharp weight loss is observed at  $200^\circ\text{C}$  and continues to  $450^\circ\text{C}$ , possible due to the large scale of

were observed, and the diffraction peaks are strong and sharp, which indicates that the crystallization is good.

From the SEM image (Fig. 6a), it is clear that after calcining and washing, the ellipsoidal morphologies and sizes of the particles are well maintained. However, the surfaces of the microparticles become significantly rough (Fig. 6b) upon this heating treatment and a large number of pores appears on the ellipsoidal particles' surface (Fig. 6c). Many large mesopores in size about 10 nm, which well dispersed in the entire microparticles, are clearly seen in the images. These microparticles exhibit a three-dimensionally interconnected framework made up of nanosized building blocks—nanoparticles—with an average size of about 50 nm.

Hydrogen reduction technology was often employed to convert the non-magnetic materials to magnetic ones [19]. However, little work has been reported about the synthesis of  $\text{Fe}_3\text{O}_4$  by using controlled oxidation method. Herein, the

direct sealed thermal decomposition of  $\text{FeCO}_3$  is introduced. The formation of  $\text{Fe}_3\text{O}_4$  can be explained on the basis that ferrous carbonate undergoes thermal decomposition to produce  $\text{FeO}$  which is then oxidized to magnetite in presence of controllable amount of oxygen.



It is easy to know that 6 mol  $\text{FeCO}_3$  could be oxidized by 1 mol  $\text{O}_2$  to yield 2 mol  $\text{Fe}_3\text{O}_4$ . Therefore, in our system, the molar ratio between the  $\text{FeCO}_3$  to the  $\text{O}_2$  is carefully controlled, and pure magnetic  $\text{Fe}_3\text{O}_4$  product was obtained.

Fig. 7 shows the XRD patterns of the obtained product. All the strong and sharp diffraction peaks in the patterns can be indexed to the face-centered cubic phase of  $\text{Fe}_3\text{O}_4$  with cell constants  $a = 8.396 \text{ \AA}$ , which are consistent with the value reported in the literature (JCPDS No. 79-0419). Fig. 8a displays the typical SEM images of the as-synthesized  $\text{Fe}_3\text{O}_4$  microcrystallites. From the image, one

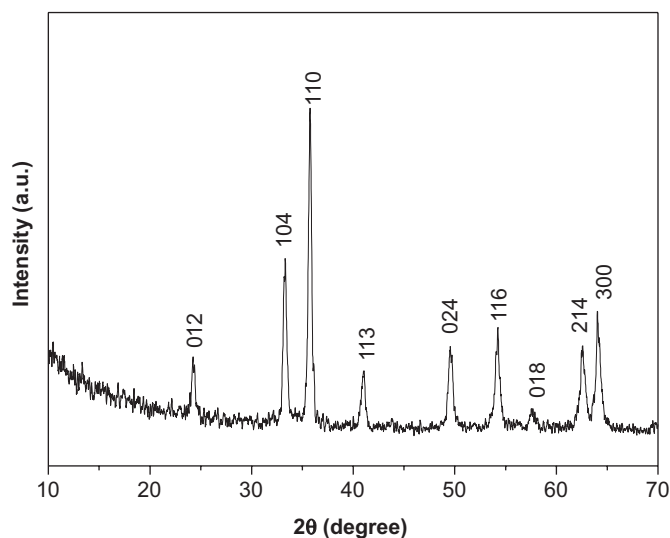


Fig. 5. The XRD patterns of the ellipsoidal  $\text{Fe}_2\text{O}_3$  microparticles.

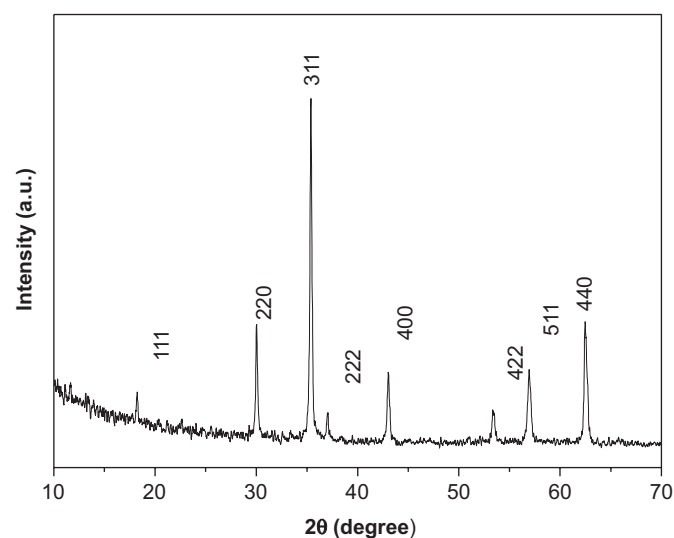


Fig. 7. XRD patterns of  $\text{Fe}_3\text{O}_4$  with ellipsoidal morphology.

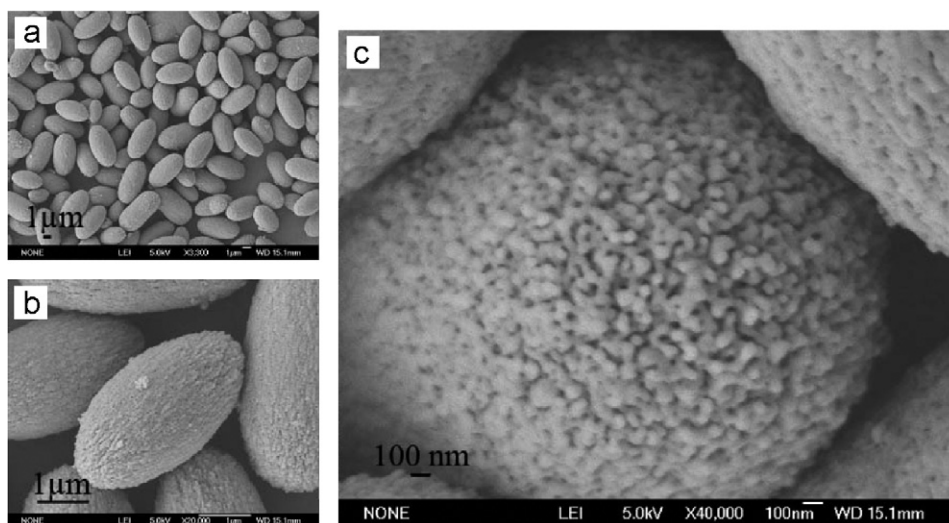


Fig. 6. The SEM image of the ellipsoidal  $\text{Fe}_2\text{O}_3$  with different magnifications.

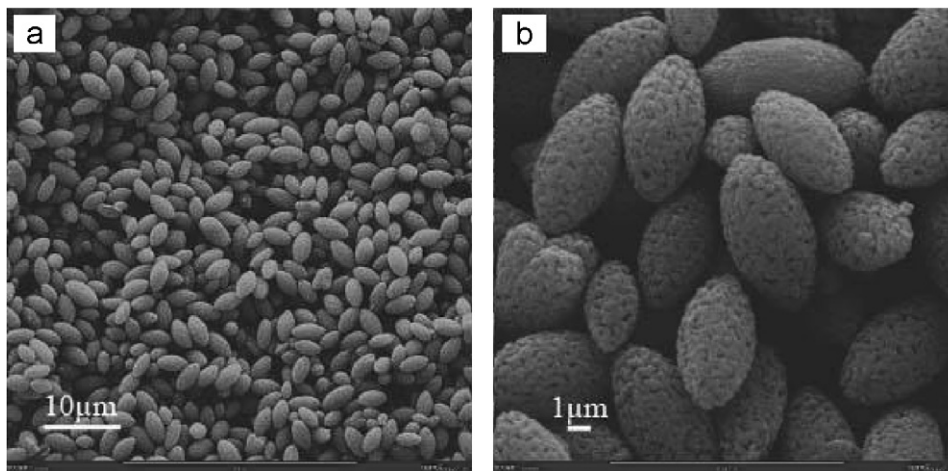


Fig. 8. SEM image of the ellipsoidal  $\text{Fe}_3\text{O}_4$  microcrystallites with low (a) and high (b) magnification.

can see that the product consists of ellipsoidal morphology with uniform size, which is similar to the  $\text{FeCO}_3$  and  $\text{Fe}_2\text{O}_3$  described above. Although  $\text{FeCO}_3$  were transformed to  $\text{Fe}_3\text{O}_4$  during the annealing process, the ellipsoidal morphology of the  $\text{Fe}_3\text{O}_4$  was almost maintained and only little  $\text{Fe}_3\text{O}_4$  nanoparticles formed during the decomposition course. However, the surfaces of the spindles become significantly rough and many of pores have been observed (Fig. 8b). Similar to the  $\text{Fe}_2\text{O}_3$ , the formation of these pores must be responsible for the decomposition of  $\text{FeCO}_3$  and release of  $\text{CO}_2$ .

The magnetic properties of the nanomaterials have been believed to be highly dependent on the sample shape, crystallinity, magnetization direction and so on. Thus, in comparison to  $\text{Fe}_3\text{O}_4$  nanoparticles, an enhanced ferromagnetic property of the as-synthesized ellipsoidal magnetite microcrystallites should be supposed. The hysteresis loop of the ellipsoidal  $\text{Fe}_3\text{O}_4$  microcrystallites at room temperature shows a ferromagnetic behavior (Fig. 9) with high saturation magnetization ( $M_s$ ), remanent magnetization ( $M_r$ ), coercivity ( $H_c$ ) values of ca. 97.5 emu/g, 19.5 emu/g, and 162.5 Oe, respectively. It is reported that one-dimensional nanostructures have increased anisotropies in both the shape anisotropy and magnetocrystalline, which exert influence on their magnetic properties. Shape anisotropy can increase the coercivity. Enhance anisotropy induces large magnetic coercivity, where the magnetic spins are preferentially aligned the long axis and their reversal to the opposite direction requires higher energies than that for spheres [20–23]. Therefore, compare to the  $H_c$  value of the bulk  $\text{Fe}_3\text{O}_4$  (115–150 Oe), the ellipsoidal  $\text{Fe}_3\text{O}_4$  microcrystallites exhibit a higher values, which may be attributed to their ellipsoidal structures.

### 3.3. Impact factors of the ellipsoidal $\text{FeCO}_3$ formation

In this synthetic route, AA is a key factor to prepare pure phase of spindle-like  $\text{FeCO}_3$ . In the absence of the AA, only  $\text{Fe}_2\text{O}_3$  nanoparticles were obtained when other

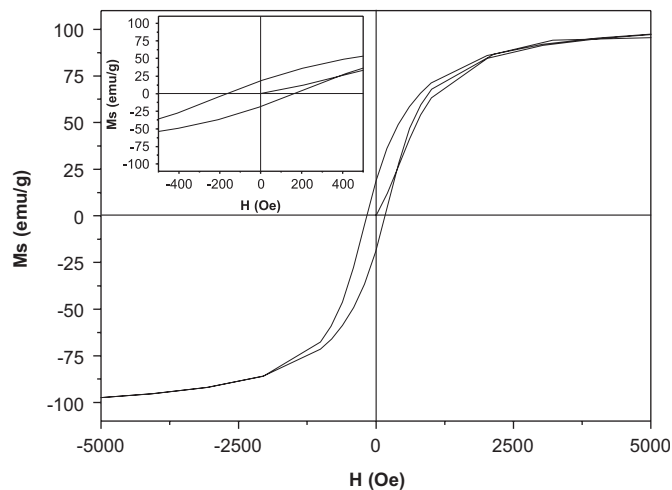


Fig. 9. Room-temperature magnetization curves of obtained ellipsoidal  $\text{Fe}_3\text{O}_4$  microcrystallites.

condition constants were fixed. This may be explained by the electrode potentials of the reactants, from which it is not difficult to find that AA is able to deoxidize  $\text{Fe}^{3+}$  to  $\text{Fe}^{2+}$  in the reaction. And then  $\text{Fe}^{2+}$  and  $\text{CO}_3^{2-}$  contribute to  $\text{FeCO}_3$ . Clearly, AA performed as the reducing reagent in this system. Though the exact role of AA played in terms of controlling crystal growth of the ellipsoidal-like product is still unclear, it is believed that AA may act as a surfactant to kinetically control the growth rates of various crystallographic facets of hexagonal  $\text{FeCO}_3$  through selectively adsorbing on these facets. The formation of the  $\text{FeCO}_3$  spindles may be attributed to the selective adsorption of AA on different crystal planes. The absorbed ligand can change the growth kinetics and surface energies of different crystal faces, which can ultimately lead to anisotropic growth of low symmetry nanostructures [24]. In the formation process of ellipsoidal-like structure, we find that AA is necessary. When other reducing reagents, such as hydrazine or other inorganic salts, are used instead of AA, we cannot get pure  $\text{FeCO}_3$ . Although pure  $\text{FeCO}_3$

was obtained when AA was substituted by glucose, the products were only irregular nanoparticles. In order to further investigate the directing role of AA, additional AA was introduced in the glucose substituting system. Interestingly, ellipsoidal-like product was obtained (Fig. 10a), which further confirmed that AA act as a structure-directing reagent to affect the growth of the ellipsoidal  $\text{FeCO}_3$ .

In addition to AA, we found that the  $\text{Na}_2\text{CO}_3$  is also a key factor in the morphology-controlling formation of  $\text{FeCO}_3$  microcrystallites. To better understand the roles of  $\text{Na}_2\text{CO}_3$  in the reaction process, we investigated in detail the effect of the amount of the added  $\text{Na}_2\text{CO}_3$  on the morphologies of the products. As it is mentioned above, when the concentration of  $\text{Na}_2\text{CO}_3$  was at 0.1715 M (the conditions mentioned in Section 2), microsized  $\text{FeCO}_3$  microcrystallites with axial ratio  $2.0 \pm 0.1$  were obtained (Fig. 3). If the concentration of  $\text{Na}_2\text{CO}_3$  decreased to 0.155 M (90% of the standard concentration of  $\text{Na}_2\text{CO}_3$ ), the axial ratio of the ellipsoidal products obtained was  $2.5 \pm 0.1$ , as indicated in Fig. 10b. However, when the concentration of  $\text{Na}_2\text{CO}_3$  was reduced to 0.0571 M (33% of the standard concentration of  $\text{Na}_2\text{CO}_3$ ), the obtained product was composed of aggregated sphere-like

structures and irregular nanoparticles, as can be seen from Fig. 10c.

In this approach, it was suggested that the source of  $\text{CO}_3^{2-}$  came from  $\text{Na}_2\text{CO}_3$ . However, how does the source of  $\text{CO}_3^{2-}$  affect the crystal growth of the final products? Here, urea was also employed as  $\text{CO}_3^{2-}$  source to fabricate  $\text{FeCO}_3$  and the morphology of the as-prepared products was studied in detail. Fig. 10d shows a general image of the obtained  $\text{FeCO}_3$  microcrystals. It clearly indicates that as-prepared products are composed of large-scale spherical microcrystallites with size in range from 20 to 40  $\mu\text{m}$  as well as some irregular big crystals. Higher magnification of SEM image (the inset of Fig. 10d) implies that the surfaces of these spheres were significantly rough. Through this experiment we find that the ellipsoidal morphology of  $\text{FeCO}_3$  cannot be obtained in the absence of the  $\text{Na}_2\text{CO}_3$ , which may be explained from the kinetic viewpoint. The nucleation rate of  $\text{FeCO}_3$  is changed when the urea was employed as the source of  $\text{CO}_3^{2-}$ ; that is to say, the reaction rate is changed, so it may affect the nanocrystal growth. Because this sealed system involves a highly non-equilibrium environment originated from the higher pressure and higher temperature, further investigation is needed to better understand the formation of these unique materials.

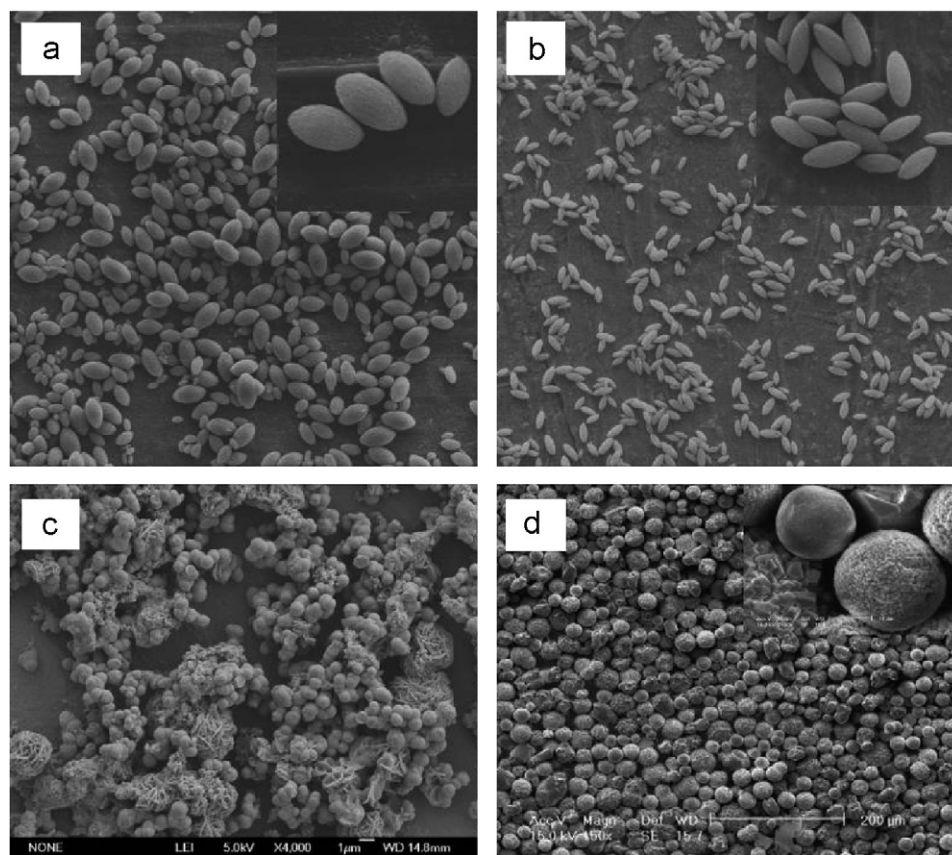


Fig. 10. SEM images of the ellipsoidal  $\text{FeCO}_3$  microcrystallites obtained at an  $[\text{AA}] = 0.02 \text{ M}$  and  $[\text{Glucose}] = 0.06 \text{ M}$ , and concentrations of  $\text{Fe}^{3+}$  of 0.057 M and  $\text{Na}_2\text{CO}_3$  of 0.1715 M (a); at an  $[\text{AA}] = 0.065 \text{ M}$  and concentrations of  $\text{Fe}^{3+}$  of 0.057 M with different  $[\text{Na}_2\text{CO}_3] = 0.155 \text{ M}$  (b) and 0.057 M (c), respectively; at an  $[\text{AA}] = 0.065 \text{ M}$  and concentrations of  $\text{Fe}^{3+}$  of 0.057 M when the urea was employed as the  $\text{CO}_3^{2-}$  source (d), at a reaction time of 3 h. The inset is the image of the product with high magnification.

#### 4. Conclusions

In summary, ellipsoidal  $\text{FeCO}_3$  microcrystals have been synthesized via an AA assisted hydrothermal process. Both the micro-sized ellipsoidal  $\text{Fe}_2\text{O}_3$  and  $\text{Fe}_3\text{O}_4$  microcrystallites can be obtained using the  $\text{FeCO}_3$  ellipsoids as sacrificial templates via direct thermal decomposition and sealed thermal decomposition for 2 h at 500 °C, respectively. In the hydrothermal process, AA performed both as reducer and structure-directing reagent, which can selectively absorb on different crystalline faces and in turn kinetically control the anisotropic growth of the microcrystals. The influence of the experimental factors such as concentration of AA and  $\text{Na}_2\text{CO}_3$  were also studied. It should be pointed out that our present understanding of forming of the mechanism of the ellipsoid microstructures is still limited, and more in-depth studies are in progress.

#### Acknowledgment

This work is supported by the Postdoctoral Fund of Chinese Academy of Sciences (No. 20060390689) and NSFC (Grant no. 10672154).

#### References

- [1] S. Mann, G.A. Ozin, *Nature* 382 (1996) 313.
- [2] H. Yang, N. Coombs, G.A. Ozin, *Nature* 386 (1997) 692.
- [3] Y. Saito, T. Matsumoto, *Nature* 392 (1998) 237.
- [4] Y. Sun, Y. Xia, *Science* 298 (2002) 2176.
- [5] J.Y. Lao, D.J. Huang, D.Z. Wang, Z.F. Ren, *Nano Lett.* 3 (2003) 235.
- [6] Z.R. Dai, Z.W. Pan, Z.L. Wang, *J. Am. Chem. Soc.* 124 (2002) 8673.
- [7] Y. Ji, X. Ma, H. Zhang, J. Xu, D. Yang, *J. Phys.: Condens. Matter* 15 (2003) 7611.
- [8] Y.Q. Zhu, W.K. Hsu, W.Z. Zhou, M. Terrones, H.W. Kroto, D.R. Walton, *Chem. Phys. Lett.* 347 (2001) 337.
- [9] R.M. Cornell, U. Schwertmann, *The Iron Oxide-Structure, Properties, Reaction, Occurrence and Uses*, VCH, Weinheim, Germany, 1996.
- [10] R.Y. Hong, T.T. Pan, H.Z. Li, *J. Magn. Magn. Mater.* 303 (2006) 60.
- [11] J. Wan, X. Chen, Z. Wang, X. Yang, Y. Qian, *J. Cryst. Growth* 276 (2005) 571.
- [12] X.G. Chen, Z.G. Zhang, X.X. Li, C.W. Shi, *Chem. Phys. Lett.* 422 (2006) 294.
- [13] G. Zou, K. Xiong, C. Jiang, H. Li, Y. Wang, S. Zhang, Y. Qian, *Nanotechnology* 16 (2005) 1584.
- [14] Z. Huang, Y. Zhang, F. Tang, *Chem. Commun.* 3 (2005) 342.
- [15] Z. Liu, D. Zhang, S. Han, C. Li, B. Lei, W. Lu, J. Fang, C. Zhou, *J. Am. Chem. Soc.* 127 (2005) 6.
- [16] H. Wang, D.W. Brandl, F. Le, P. Nordlander, N.J. Halas, *Nano Lett.* 6 (2006) 827.
- [17] H. Naono, R. Fujiwara, *J. Colloid Interface Sci.* 73 (1980) 406.
- [18] S. Lian, E. Wang, Z. Kang, Y. Bai, L. Gao, M. Jiang, C. Hu, L. Xu, *Solid State Commun.* 129 (2004) 485.
- [19] Y.C. Sui, R. Skomski, K. Sorge, D. Sellmyer, *J. Appl. Phys.* 95 (2004) 11.
- [20] S.J. Park, S. Kim, S. Lee, Z.G. Kim, K. Char, J. Hyeon, *J. Am. Chem. Soc.* 122 (2000) 8581.
- [21] F. Dumestre, B. Chaudret, C. Amine, M.C. Fromen, M.J. Casanove, P. Renaud, P. Zurcher, *Angew. Chem. Int. Ed.* 41 (2002) 4286.
- [22] L. Néel, In *Low-Temperature Physics*; C. Dewitt, B. Dreyfus, P.G. Degennes, Gordon and Beach: London, (1962) 411.
- [23] W.S. Seo, H.H. Jo, K. Lee, B. Kim, S.J. Oh, T. Park, *Angew. Chem. Int. Ed.* 43 (2004) 1115.
- [24] V.F. Puentes, D. Zanchet, C.K. Erdonmez, A.P. Alivisatos, *J. Am. Chem. Soc.* 124 (2002) 12874.